Effect of Sn on the Reactivity of Cu Surfaces

Amit A. Gokhale, George W. Huber, James A. Dumesic, and Manos Mavrikakis*

Department of Chemical and Biological Engineering, University of Wisconsin—Madison, 1415 Engineering Drive, Madison, Wisconsin 53706

Received: May 9, 2004; In Final Form: June 24, 2004

Periodic, density functional theory (DFT-GGA) calculations, using PW91 (self-consistently) and RPBE functionals, have been employed to determine preferred binding sites, adsorbate structures, and binding energies for the adsorption of atomic (H, N, O, S, and C), molecular (NO and CO), and radical (OH) species on Cu(111) and CuSn(0001) alloy surfaces. Our results indicate the following order in the binding energies from the least to the most strongly bound: NO < CO < H < OH < N < O < S < C for Cu-terminated CuSn(0001). On Cu(111), the corresponding relative order of adsorbates from the least strongly bound to the most strongly bound is CO < NO < H < OH < N < O < S < C. On the Sn-terminated CuSn(0001) surface, CO does not adsorb and the relative order of adsorbates from the least strongly bound to the most strongly bound is NO < H < OH < N < S < O < C. For all adsorbates, the binding on Cu-terminated CuSn(0001) is stronger than on Cu(111), resulting from a combination of electronic and strain effects caused by the addition of Sn to Cu. CO dissociation is endothermic on Cu-terminated CuSn(0001) and Cu(111) surfaces, while CO oxidation is exothermic on these surfaces. OH dissociation is endothermic on all three surfaces. On all surfaces studied, thermodynamics of NO decomposition are much more favorable than those of CO and OH dissociation on the corresponding surfaces. Our microcalorimetric studies of the interaction of NO with Cu/SiO_2 and Cu_6Sn_5/SiO_2 samples give initial heats of 270 (2.80 eV) and 130 (1.35 eV) kJ/mol, respectively. These values correspond to the decomposition of NO to give adsorbed oxygen plus gaseous N_2 on Cu/SiO_2 and adsorbed oxygen plus gaseous N_2O on the Sn-terminated phase of Cu_6Sn_5/SiO_2.

Introduction

Copper-based catalysts are used for a wide variety of processes, such as methanol synthesis,[1−7] methanol reforming,[8−10] and low temperature water gas shift (WGS).[9,11−13] Copper-based catalysts are also used in the automobile industry,[14,15] as well as for acrolein synthesis, dehydrogenation of cycloalkanes, and dehydrogenation of alcohols.[14−16] Accordingly, numerous experimental and theoretical studies have been conducted to understand the fundamental surface chemistry of copper, in terms of the adsorption of species such as hydrogen,[17,18] oxygen,[18−20] carbon,[21] hydroxyl,[18,22] CO, and NO.[5,20,23]

Here, we present a systematic study of the structures and energetics of monatomic (H, O, N, S, and C) and diatomic (CO, NO, and OH) species on Cu(111). We use periodic, self-consistent density funtional theory (DFT) calculations to determine preferred binding sites and binding energies for the adsorbed species. Also, on the basis of the binding energies of the adsorbates at the high symmetry sites, we estimate the diffusion barriers for these adsorbates on the surfaces considered. These results form the basis for documenting the effects of adding modifiers such as tin on the surface chemistry. In this respect, we report results from DFT calculations for the various adsorbates on surfaces of Cu alloyed with Sn, in particular Cu-terminated CuSn(0001) and Sn-terminated CuSn(0001) surfaces. We chose tin as a modifying agent because this additive is used widely in heterogeneous catalysis applications, e.g., to alter hydrogenolysis and isomerization reactions of paraffins on metal catalysts.[24−27] Because of its oxophilic nature, Sn may also participate in catalytic reactions involving oxygen-containing reactants such as alcohols, carboxylic acids, and esters.[28−31] In addition, Cu supported on SnO_2 appears to be a good catalyst for CO oxidation.[32] Finally, we use the findings from our DFT calculations to interpret experimental results from microcalorimetric measurements of the heats of interaction of NO and CO with silica-supported Cu and CuSn catalysts.

Experimental Section

A silica-supported Cu catalyst containing 11.1 wt % Cu was prepared by incipient wetness impregnation of SiO_2 (Cab-o-sil, Grade EH-5, Cabot) with an aqueous copper(II) nitrate trihydrate solution, followed by drying at 373 K for 14 h. Another Cu/SiO_2 catalyst was prepared by the same method containing 4.7 wt % Cu, and this material was then impregnated with a Sn (tributyl tin acetate, Aldrich) solution in ethanol and dried again at 373 K for 14 h to prepare a Cu_6Sn_5/SiO_2 catalyst. Prior to characterization, the catalysts were reduced in flowing H_2 at 673 K with a 2 h hold preceded by an 8 h ramp from 298 to 673 K. The Cu, Sn, and Si contents of the catalysts were measured by inductively coupled plasma emission spectroscopy with a Perkin-Elmer Plasma 400 ICP Emissions Spectrometer.

Mössbauer spectroscopy and X-ray diffraction (XRD) were used to confirm that Cu_6Sn_5 is the dominant phase in the Cu_6Sn_5/SiO_2 catalyst. Mössbauer spectra were collected at 300 K with an Austin Science Associates model S-600 Mössbauer spectrometer operated in constant acceleration mode with a 20 mCi γ-ray $Ca^{119}SnO_3$ source. A glass cell with thin windows was used for treatments and to collect the Mössbauer data. XRD scans were collected with a Cu Kα source on a Scintag PADV X-ray Diffractometer operating at 40.0 mA and 35.0 kV.

* To whom correspondence should be addressed. Tel: +1-608-262-9053. Fax: +1-608-262-5434. E-mail: manos@engr.wisc.edu.

10.1021/jp048013c CCC: $27.50
Published on Web 08/19/2004

Microcalorimetric measurements of NO adsorption were performed at 300 K using a Setaram BT2.15D heat-flux calorimeter. Details of the procedure for microcalorimetric measurements may be found elsewhere.[33,34] In short, each sample was treated first in flowing H_2 [200 cm^3(STP)/min] at 673 K, followed by treatment in flowing helium for 2 h at the same temperature. The sample was then torch sealed under He in a Pyrex capsule, and the capsule was loaded into a set of calorimetric cells. After the sample and cell reached thermal equilibrium with the calorimeter, the capsule was broken and microcalorimetric measurements were made by sequentially introducing small doses (ca. 1 μmol/g) of NO onto the sample. The heat signal was recorded as a function of time, and this signal was integrated to obtain the energy released per dose. Volumetric measurements were made to determine the amount of gas adsorbed during the dose, using the dosing pressure, equilibrium pressure, system volumes, and temperature.

Measurements were also made of the irreversible uptakes of CO and NO at 300 K, as well as the N_2O uptake at 370 and 300 K for the Cu_6Sn_5/SiO_2 catalyst, using a standard gas adsorption apparatus described elsewhere.[35] The N_2O measurements were made by exposing the reduced catalyst to N_2O at 370 or 300 K for 20 min, followed by condensing the N_2O at 77 K to measure the residual N_2 pressure.

DFT Methods

All calculations were carried out using a planewave total energy code (DACAPO).[36,37] Four layer slabs of Cu(111) and CuSn(0001) were used, periodically repeated in a super cell geometry with five equivalent layers of vacuum between any two successive metal slabs. CuSn has a NiAs type layered structure; hence, both Cu-terminated and Sn-terminated surfaces were considered. In all cases, a 2×2 unit cell was used, corresponding to a surface coverage of 0.25 ML. Adsorption was allowed on only one of the two exposed surfaces, and the electrostatic potential was adjusted accordingly.[38] The calculations were performed by relaxing the top two layers of the slabs, whereas spin polarization was implemented as needed (e.g., adsorption of NO). Ionic cores were described by ultrasoft pseudopotentials,[39] and the Kohn−Sham one-electron valence states were expanded in a basis of plane waves with a kinetic energy below 25 Ry. The surface Brillouin zone was sampled at 18 special **k**-points.[40] In all cases, convergence with respect to the **k**-point set and the number of metal layers was confirmed. The exchange correlation energy and potential were described by two generalized gradient approximations, self-consistently with GGA-PW91[41,42] and non-self-consistently with RPBE.[36] The self-consistent PW91 density was determined by iterative diagonalization of the Kohn−Sham Hamiltonian, Fermi population of the Kohn−Sham states ($k_BT = 0.1$ eV), and Pulay mixing of the resulting electronic density.[43] All total energies have been extrapolated to $k_BT = 0$ eV. The calculated lattice constant for bulk CuSn, 4.21 Å, is less than 1% off from the experimental value of 4.19 Å.[44] Similarly, the lattice constant calculated for bulk Cu is 3.66 Å,[5,19,45,46] which compares well with the experimentally determined value of 3.61 Å.[47] Here, we note that the calculated lattice constant for CuSn and Cu points to an expansion of the Cu lattice by 15% due to the addition of Sn. Accordingly, we have studied adsorption on a 15% stretched Cu(111) slab, analogous to that studied previously by Xu and Mavrikakis,[19] in order to evaluate the isolated strain effect in the CuSn alloy.

Diffusion barriers of various adsorbates have been estimated by comparing binding energies of the corresponding adsorbate at various high symmetry surface sites. This approach has been followed in the past[48,49] and has been shown to yield fairly accurate diffusion barrier estimates, when compared to more accurate, but at the same time, much more expensive calculations, for instance, by using the nudged elastic band method.[50]

Electron density difference plots were generated for selected adsorbates to analyze the electronic structure of various bonds. For this purpose, we plotted the electron density difference defined as:

$$\text{electron density difference} = \{\text{electron density of (adsorbate + slab)}\} - \{\text{electron density of clean slab}\} - \{\text{electron density of the adsorbate in the gas phase}\}$$

where the electronic density for the clean slab was obtained by removing the adsorbate and freezing the atoms in their positions, to account for the adsorbate-induced surface reconstruction effects.

Experimental Results

Mössbauer spectroscopy and XRD studies were carried out to determine the extent to which CuSn alloys were, in fact, present on the Cu_6Sn_5/SiO_2 sample of this work. In addition, we conducted experimental studies of CO, N_2O, and NO chemisorption and NO microcalorimetry on Cu/SiO_2 and Cu_6Sn_5/SiO_2 samples to provide comparisons with predictions from DFT calculations.

The results from in situ Sn Mössbauer spectroscopy and XRD scans of the Cu_6Sn_5/SiO_2 sample showed that the major phase is, in fact, Cu_6Sn_5. For this sample, we find that the amount of irreversible CO adsorption at 300 K is very small (0.12 μmol/g). In contrast, a large amount of oxygen can be deposited onto this Cu_6Sn_5/SiO_2 catalyst by N_2O decomposition at 370 K, such that the ratio of O atom uptake to irreversible CO adsorption is equal to 375:1. This behavior suggests that CO does not adsorb strongly on Cu_6Sn_5. At 300 K, the amount of O atom uptake from N_2O decomposition on Cu_6Sn_5/SiO_2 catalyst is only 0.56 μmol/g, suggesting that N_2O dissociation on the supported catalyst is negligible at lower temperatures. NO adsorption uptakes on both Cu/SiO_2 as well as Cu_6Sn_5/SiO_2 catalysts are significant (72 and 12 μmol/g, respectively). NO did not adsorb on a pure SiO_2 sample at room temperature as determined from a blank microcalorimetry experiment.

Figure 1a,b shows plots of the differential heat vs the NO uptake for the Cu/SiO_2 and Cu_6Sn_5/SiO_2 samples, respectively. When NO is initially dosed into the cell for the microcalorimetry experiments, a residual gas pressure appears, which corresponds to approximately half the amount of NO originally dosed into the cell. For the initial doses (as shown with red in Figure 1a,b), it is assumed that NO dissociates to form adsorbed O for both catalysts and gas phase N_2 or N_2O for the Cu/SiO_2 and Cu_6Sn_5/SiO_2 catalysts, respectively. At higher coverages, as shown with blue in Figure 1a,b, it is assumed that NO adsorbs molecularly. Open symbols in Figure 1a show a transition between dissociative and molecular adsorption of NO, and we have assumed that in this transition region, half the NO dissociates and the other half adsorbs molecularly. Thus, in Figure 1a,b, the differential heat is plotted vs the total amount of NO that has either dissociated or adsorbed. Later in this paper, we will show that these assumptions are consistent with the results from DFT calculations.

We find the initial heat of reaction to be 270 kJ/mol (2.80 eV) on Cu/SiO_2 and 130 kJ/mol (1.35 eV) for Cu_6Sn_5/SiO_2 at low coverages (see Figure 1a,b). At higher coverages (blue

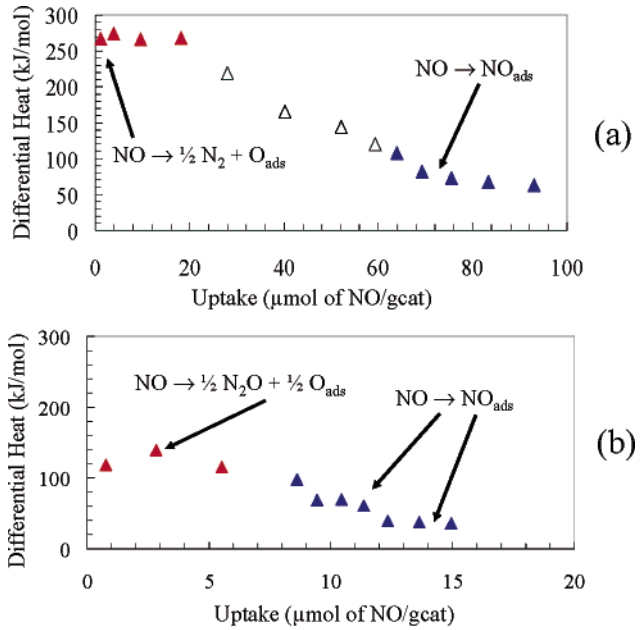

Figure 1. Differential heat vs uptake of NO adsorption on (a) Cu/SiO_2 and (b) Cu_6Sn_5/SiO_2 at 300 K. Symbols in red indicate the heat of reaction for NO dissociation to O_{ads} plus gas phase N_2 (for Cu) or N_2O (for Cu_6Sn_5). Symbols in blue indicate the heat of molecular NO adsorption. Open symbols show a transition between these two regimes in which it is assumed that half the NO adsorbs dissociatively and half adsorbs molecularly. Note that 1 eV = 96.5 kJ/mol.

closed symbols in Figure 1a), a plateau is seen for the Cu/SiO_2 substrate at 68 kJ/mol (0.70 eV). This plateau, as will be shown later, is associated with the molecular adsorption of NO on the surface. Similar plateaus can be seen on the Cu_6Sn_5/SiO_2 substrate at 69 (0.72 eV) and 38 (0.39 eV) kJ/mol (Figure 1b).

DFT Results and Discussion

A summary of the calculated binding energies for atomic, molecular, and radical adsorbates on the Cu-terminated CuSn(0001), Sn-terminated CuSn(0001), and Cu(111) surfaces is presented in Table 1, while the estimated diffusion barriers for the adsorbates on these surfaces are listed in Table 2. Binding energies are presented for both PW91 and RPBE functionals, with the later given in square brackets. We compare our results on Cu(111) with those of previous studies, both experimental and theoretical. No previous studies have been conducted on CuSn(0001) surfaces for comparison. The nature of the bond between the adsorbate and the metal is probed for selected adsorbates on all three surfaces using electron density difference plots. To study the effect of strain due to alloying Cu with Sn, the binding energies of adsorbates on Cu(111) and Cu-terminated CuSn(0001) are compared to those on 15% stretched Cu(111).

Adsorption of Atoms

Atomic hydrogen is the least strongly bound atom among those we studied on all three surfaces. For the Cu-terminated CuSn(0001) slab, H adsorbs most strongly at the fcc site with a binding energy of −2.97 [−2.69] eV (Table 1). A noticeable lateral surface reconstruction is found, with the surface Cu atoms being directed radially inward, toward the adsorbed H. The geometric parameters for this configuration are presented in Table 3, while Figure 2 shows a schematic representation of the corresponding structural parameters. Figure 3a,f,k shows the adsorbed state of H on Cu-terminated CuSn(0001), Sn-terminated CuSn(0001), and Cu(111), respectively. For the Cu-terminated CuSn(0001) surface, the barrier for H diffusion is estimated around 1.00 [0.90] eV (Table 2). For the Sn-terminated CuSn(0001) surface, the most favorable site is the top site with a binding energy of −1.91 [−1.80] eV, which is significantly lower than the binding energy on the Cu-terminated CuSn(0001) surface. The estimated H diffusion barrier is less than 0.1 eV (Table 2), suggesting higher mobility of atomic hydrogen on the Sn-terminated CuSn(0001) surface than the Cu-terminated CuSn(0001) surface. The binding energy of hydrogen on Cu(111) is intermediate between the values on the Cu-terminated and Sn-terminated CuSn(0001) surfaces, with the fcc site being the most favored site. The binding energy of atomic hydrogen at this site is −2.39 [−2.23] eV, which is 0.58 [0.46] eV less than on Cu-terminated CuSn(0001). This difference suggests that addition of Sn enhances the binding of atomic hydrogen to copper. A possible explanation for this enhancement may lie with the strain induced in the surface by the presence of Sn. The surface atoms in Cu-terminated CuSn(0001) slab are stretched by about 15% as compared to Cu(111). Similar increases in binding energy for highly stretched surfaces have been calculated previously for CO and NO on Ru(0001),[51,52] CO on Cu(111),[45] and O on Cu(111).[19,53] Indeed, increasing the lattice constant of pure copper by 15% leads to a significant increase in the binding strength of H on Cu(111) (Table 4 and Figure 4). The binding energy on the 15% stretched Cu(111) surface is −2.52 [−2.31] eV, suggesting that both the strain and the electronic effect due to the addition of Sn play a role in increasing the binding strength of H on copper.

Our assignment of the best site for atomic hydrogen adsorption on Cu(111) differs from the previous HREELS/IRAS study by McCash et al.[54] but is concurrent with the IRAS study by Lamont et al.[55] and HREELS studies.[56] A number of theoretical studies[17,57,58] also suggest that the fcc site is the preferred site for H adsorption on Cu(111). Previous DFT studies using a cluster approach[18] have determined the binding energy of atomic hydrogen on Cu(111) to be −2.23 eV. Periodic DFT calculations predict binding energies of about −2.40 eV[5,36] in good agreement with our findings (−2.39 [−2.23] eV). Our calculations indicate that the distance between the hydrogen atom and the Cu(111) slab is 0.89 Å (see Table 3), in good agreement with the value of 0.90 Å determined by Koper and van Santen.[18]

The next least strongly bound atom from those studied here is nitrogen. The favored binding site for N on Cu-terminated CuSn(0001) is the hcp site, with a binding energy of −4.27 [−3.92] eV (Table 1). The diffusion barrier for N on this surface is estimated to be 0.85 [0.71] eV (Table 2). The geometric parameters for the hcp site are presented in Table 3. The site preference and the approximate surface reconstruction are similar to that for adsorption of O atoms, shown in Figure 3b. For the Sn-terminated CuSn(0001) surface, the most favorable site for nitrogen adsorption is the hcp site with a binding energy of −3.37 [−3.11] eV. The surface reconstruction in this case is more extensive than that for the Cu-terminated CuSn(0001) surface (Table 3). The estimated diffusion barrier (0.81 [0.89] eV) is similar to that on the Cu-terminated surface. On Cu(111), the strongest nitrogen adsorption is seen at the fcc site with a binding energy of −3.25 [−2.80] eV. This value agrees well with the binding energy determined by Bogicevic and Hass[20] (−3.85 eV) for a coverage of 1/9 ML. They also found the fcc site to be the best site for N adsorption on Cu(111). The geometric parameters for this configuration are presented in Table 3. The activation energy for diffusion of nitrogen on

TABLE 1: Binding Energies of Adsorbates on Relaxed Cu-Terminated CuSn(0001), Sn-Terminated CuSn(0001), and Cu(111) Surfaces[a]

Atomic Adsorbates					
	binding energy (eV) PW91 [RPBE]				
surface	top	bridge	hcp	fcc	best site
			Hydrogen		
Cu-terminated CuSn(0001)	−1.84 [−1.62]	−2.61 [−2.39]	−1.61 [−1.49]	**−2.97 [−2.69]**	fcc
Sn-terminated CuSn(0001)	**−1.91 [−1.80]**	−1.51 [−1.48]	−1.83 [−1.70]	−1.56 [−1.46]	top
Cu(111)	−1.76 [−1.64]	−2.24 [−2.09]	−2.38 [−2.21]	**−2.39 [−2.23]**	fcc
			Nitrogen		
Cu-terminated CuSn(0001)	−0.76 [−0.53]	−3.42 [−3.21]	**−4.27 [−3.92]**	−3.38 [−2.94]	hcp
Sn-terminated CuSn(0001)	−0.99 [−0.79]	−2.56 [−2.22]	**−3.37 [−3.11]**	−2.93 [−2.72]	hcp
Cu(111)	−0.97 [−0.67]	−2.89 [−2.45]	−3.15 [−2.72]	**−3.25 [−2.80]**	fcc
			Oxygen		
Cu-terminated CuSn(0001)	−2.53 [−2.18]	−4.92 [−4.45]	**−5.03 [−4.57]**	−4.86 [−4.31]	hcp
Sn-terminated CuSn(0001)	−3.50 [−3.14]	−4.22 [−3.76]	−4.19 [−3.74]	**−4.36 [−3.94]**	fcc
Cu(111)	−2.37 [−1.94]	−3.74 [−3.35]	−4.17 [−3.58]	**−4.29 [−3.69]**	fcc
			Sulfur		
Cu-terminated CuSn(0001)	−2.92 [−2.64]	−4.33 [−3.97]	**−5.06 [−4.68]**	−4.89 [−4.46]	hcp
Sn-terminated CuSn(0001)	−3.10 [−2.85]	−3.01 [−2.68]	**−3.76 [−3.38]**	−3.48 [−3.17]	hcp
Cu(111)	−3.05 [−2.63]	−4.12 [−3.70]	−4.26 [−3.75]	**−4.33 [−3.80]**	fcc
			Carbon		
Cu-terminated CuSn(0001)	−2.06 [−1.72]	−4.51 [−4.09]	**−5.14 [−4.75]**	−4.49 [−4.01]	hcp
Sn-terminated CuSn(0001)	−1.70 [−1.43]	−3.73 [−3.48]	**−4.51 [−4.23]**	−4.16 [−3.87]	hcp
Cu(111)	−2.48 [−2.08]	−4.15 [−3.65]	−4.36 [−3.85]	**−4.41 [−3.90]**	fcc
Molecular and Radical Adsorbates					
	binding energy (eV) PW91 [RPBE]				
surface	top	bridge	hcp	fcc	best site
			Nitric Oxide (NO)		
Cu-terminated CuSn(0001)	−0.83 [−0.39]	**−1.19 [−0.73]**[b]	−1.03 [−0.54]	−0.82 [−0.34]	bridge
Sn-terminated CuSn(0001)	−0.46 [−0.25][b]	**−0.65 [−0.35]**[b]	−0.09 [0.00]	−0.63 [−0.33]	bridge
Cu(111)	−0.55 [−0.13]	−0.90 [−0.39]	−0.98 [−0.44]	**−1.03 [−0.47]**	fcc
			Carbon Monoxide (CO) (Adsorption on Sn-Terminated CuSn(0001) Surface Is Not Exothermic)		
Cu-terminated CuSn(0001)	−1.10 [−0.74]	−1.02 [−0.61]	−0.40 [0.00]	**−1.20 [−0.62]**	fcc [top]
Cu(111)	−0.73 [−0.37]	−0.79 [−0.36]	**−0.84 [−0.39]**	**−0.84 [−0.39]**	hcp/fcc
			Hydroxyl Radical (OH)		
Cu-terminated CuSn(0001)	−2.54 [−2.15][b]	−3.32 [−2.81][b]	−3.19 [−2.67]	**−3.51 [−2.87]**	fcc
Sn-terminated CuSn(0001)	**−2.76 [−2.37]**[b]	−2.60 [−2.12][b]	−2.63 [−2.13]	−2.32 [−1.86]	top
Cu(111)	−2.19 [−1.77][b]	−2.65 [−2.10]	−2.79 [−2.21]	**−2.85 [−2.26]**	fcc

[a] The PW91 [RPBE] binding energies are shown. Best sites based on PW91 binding energies correspond to the boldfaced entries. The reference zero corresponds to the gas phase species at infinite separation from the corresponding slabs. [b] Indicates a tilted state.

TABLE 2: PW91 [RPBE] Estimates for the Diffusion Barriers for Atomic, Molecular, and Radical Species on Cu-Terminated CuSn(0001), Sn-Terminated CuSn(0001), and Cu(111)

	diffusion barrier on		
adsorbate	Cu-terminated CuSn(0001) (eV)	Sn-terminated CuSn(0001) (eV)	Cu(111) (eV)
H	1.00 [0.90]	0.08 [0.10]	0.15 [0.14]
N	0.85 [0.71]	0.81 [0.89]	0.36 [0.35]
O	0.11 [0.14]	0.14 [0.18]	0.55 [0.34]
S	0.73 [0.71]	0.66 [0.53]	0.21 [0.10]
C	0.63 [0.66]	0.78 [0.75]	0.26 [0.25]
NO	0.16 [0.19]	0.02 [0.02]	0.13 [0.08]
CO	0.10 [0.12]	CO does not adsorb	0.05 [0.02]
OH	0.19 [0.14]	0.13 [0.24]	0.20 [0.16]

TABLE 3: Vertical Distance between Adsorbates and the Plane of the Three Atoms Defining the Corresponding Site (d_{Cu-A} or d_{Sn-A}), and Metal−Metal Bond Length within the Surface Plane (d_{Cu-Cu} or d_{Sn-Sn})[a]

	Cu-terminated CuSn(0001)		Sn-terminated CuSn(0001)		Cu(111)	
adsorbate	d_{Cu-A} (Å)	d_{Cu-Cu} (Å)	d_{Sn-A} (Å)	d_{Sn-Sn} (Å)	d_{Cu-A} (Å)	d_{Cu-Cu} (Å)
H	0.98	2.51	1.76	4.21	0.89	2.60
N	0.23	3.39	0.43	3.85	1.05	2.67
O	0.27	3.56	0.96	3.38	1.18	2.68
S	0.89	3.67	1.08	4.09	1.62	2.66
C	0.28	3.34	0.37	3.88	1.04	2.67
NO	1.01	3.50	1.52	4.01	1.33	2.64
CO	1.32	2.65	CO does not adsorb		1.44	2.57
OH	1.33	2.76	2.03	4.21	1.38	2.66

[a] A schematic representation is given in Figures 2 and 3. On a clean Cu-terminated or Sn-terminated CuSn(0001) surface, $d_{Cu-Cu} = d_{Sn-Sn} = 4.21$ Å, and on a clean Cu(111) surface, $d_{Cu-Cu} = 2.59$ Å.

Cu(111) is estimated to be 0.36 [0.35] eV (Table 2), which is much lower as compared to that on both of the CuSn(0001) surfaces, suggesting that atomic nitrogen is much more mobile on Cu(111) than on CuSn(0001) surfaces. This N diffusion barrier estimate agrees well with the estimate of 0.28 eV for N on Cu(111), calculated by Bogicevic and Hass[20] for a 1/9 ML coverage using the PW91 functional.

To explain the binding characteristics of N on the three surfaces of this study, we have generated the density difference plots for N adsorption at the hcp site on Cu-terminated CuSn(0001), Sn-terminated CuSn(0001), and Cu(111) (Figure 5). We note here that the hcp site is not the best site for N adsorption on Cu(111); however, the binding strength at the hcp site isnot significantly different from that at the best (fcc) site (see Table 1). We can attribute the increased binding energy on CuSn(0001) surfaces to the stronger interactions between N and both the first and the second layer Cu and Sn atoms, as opposed to N interacting almost exclusively with the first layer Cu atoms in Cu(111). Furthermore, charge transfer is more facile between Cu and N rather than between Sn and N. However, strain

TABLE 4: PW91 [RPBE] Binding Energies and Site Preferences (Based on PW91) for Adsorbates, on Relaxed Cu(111), 15% Stretched Cu(111), and Copper-Terminated CuSn(0001) Surfaces[a]

	PW91 [RPBE] binding energy of adsorbates (eV)					
	Cu(111) slab		15% stretched Cu(111) slab		Cu-terminated CuSn(0001) slab	
species	binding energy PW91 [RPBE] (eV)	site	binding energy PW91 [RPBE] (eV)	site	binding energy PW91 [RPBE] (eV)	site
H	−2.39 [−2.23]	fcc	−2.52 [−2.31]	hcp	−2.97 [−2.69]	fcc
N	−3.25 [−2.80]	fcc	−4.38 [−3.88]	hcp	−4.27 [−3.92]	hcp
O	−4.29 [−3.69]	fcc	−5.08 [−4.45]	hcp	−5.03 [−4.57]	hcp
S	−4.33 [−3.80]	fcc	−4.80 [−4.35]	fcc	−5.06 [−4.68]	hcp
C	−4.41 [−3.90]	fcc	−6.12 [−5.60]	fcc	−5.14 [−4.75]	hcp
NO	−1.03 [−0.47]	fcc	−1.21 [−0.63]	fcc/hcp	−1.19 [−0.73]	bridge
CO	−0.84 [−0.39]	fcc/hcp	−0.99 [−0.58]	hcp	−1.20 [−0.74]	fcc
OH	−2.85 [−2.26]	fcc	−3.34 [−2.82]	fcc	−3.51 [−2.87]	fcc

[a] Reference zero corresponds to gas phase species at infinite separation from the corresponding slabs.

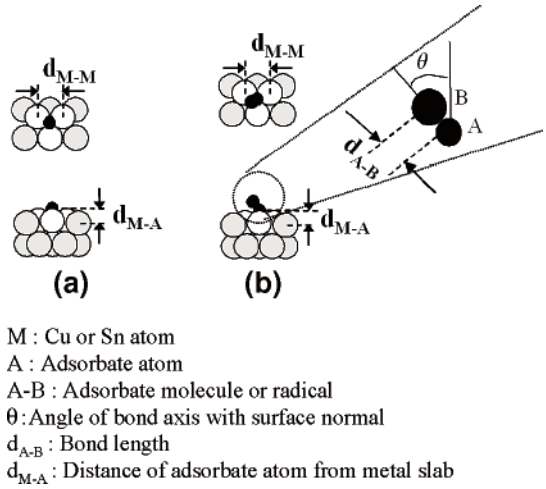

Figure 2. Schematic representation of top and side views of the atomic and diatomic adsorbates on 3-fold sites of Cu(111) and CuSn(0001). (a) Atomic adsorbates. (b) Diatomic (molecular and radical) adsorbates. Enlarged view of the diatomic adsorbate is also shown to indicate the detailed geometric aspects. Geometrical parameters are listed in Tables 3 and 5.

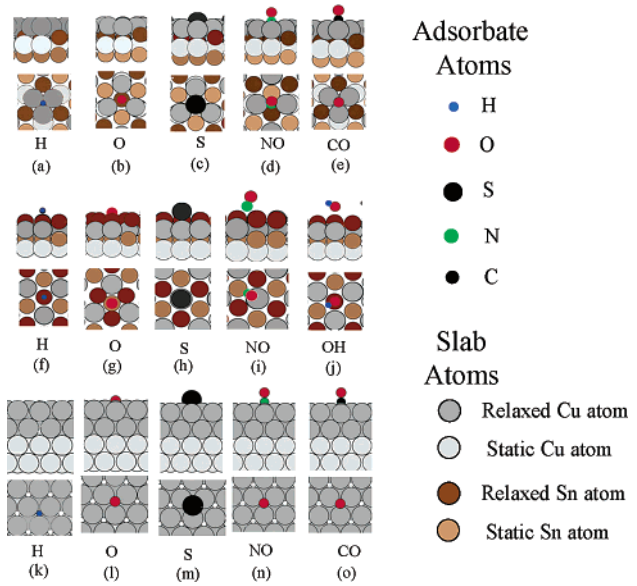

Figure 3. Preferred binding modes for selected adsorbates on Cu-terminated CuSn(0001): (a) H fcc, (b) O hcp, (c) S hcp, (d) NO bridge, (e) CO fcc; Sn-terminated CuSn(0001): (f) H top, (g) O fcc, (h) S hcp, (i) NO bridge, (j) OH top; Cu(111): (k) H fcc, (l) O fcc, (m) S fcc, (n) NO fcc, (o) CO fcc. Top and bottom panels provide a cross-section and an on-top view, respectively, of each binding state. Only representative surface reconstructions and orientations for the adsorbates at the high-symmetry sites are shown. For additional details for all adsorbates studied, see Tables 1, 3, and 5.

appears to be the main cause for the higher binding energy of the N on the Cu-terminated CuSn(0001) surface as compared to the Cu(111). As seen from Figure 4 and Table 4, N adsorption is almost as favored on the 15% stretched Cu(111) surface as it is on Cu-terminated CuSn(0001) surface. Table 4 also shows that N binds strongest on stretched Cu(111) surface and Cu-terminated CuSn(0001) surface at the hcp site, whereas on the unstretched Cu(111) surface it prefers the fcc site. These similarities in the binding energies and the site preference of N on the stretched Cu(111) and the Cu-terminated CuSn(0001) surfaces clearly point to strain being the major factor for enhancement of binding energy of N on the Cu-terminated CuSn(0001) surface. It is this strain that allows for the interaction of the adsorbed N atom with the second layer Sn atom, as seen in Figure 5.

The favored binding site for atomic oxygen on Cu-terminated CuSn(0001) is the hcp site. The binding energy at this site is −5.03 [−4.57] eV (Table 1). Previous periodic DFT studies comparing O adsorption on Pt(111) and $Pt_3Sn(111)$[27] suggest that O atoms tend to aggregate close to Sn atoms on Pt_3Sn-(111). The preference of the hcp site for the adsorption of atomic oxygen on Cu-terminated CuSn(0001) agrees well with this observation. On Sn-terminated CuSn(0001) and Cu(111), the binding energies of atomic oxygen are comparable. On these surfaces, O shows preference for the fcc site. The binding energies of O on the Sn-terminated CuSn(0001) and Cu(111) surfaces are −4.36 [−3.94] and −4.29 [−3.69] eV, respectively. The binding energy of O on Cu(111) calculated here is identical to that determined by a previous periodic DFT study.[19] The binding energy of O on Cu(111) determined by Hammer et al.[59] (−4.50 eV) also agrees with our results, considering that LDA pseudopotentials were used in that study. Our site preference on Cu(111) also agrees well with these studies.[19,59] Diffusion barriers for oxygen on the Cu-terminated CuSn(0001) and Sn-terminated CuSn(0001) surfaces are estimated to be 0.11 [0.14] and 0.14 [0.18], respectively. These values are much lower than that on Cu(111) (0.55 [0.34] eV; see Table 2). Bogicevic and Haas[20] using the PW91 functional, estimated the O diffusion barrier on Cu(111) to be 0.37 eV for 1/9 ML coverage. The activation energy for O diffusion on Cu(111) estimated here is higher, most probably because our calculations are performed at a higher coverage (1/4 ML) where repulsion between adsorbed species is expected to be higher. The geometric parameters for oxygen adsorption on Cu(111) are given in Table 3 and depicted in Figure 3b,g,l. The distance of the oxygen atom from the Cu(111) slab is 1.18 Å. This value compares well with the values

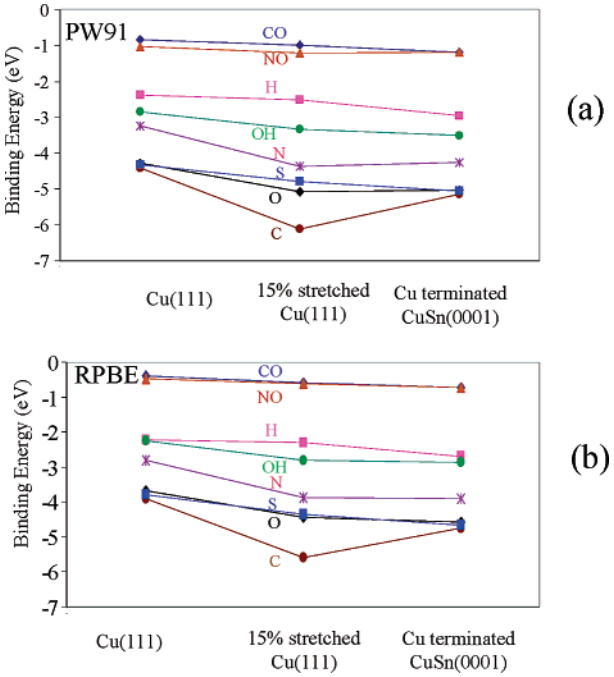

Figure 4. Binding energies of all adsorbates at their preferred sites, studied on Cu(111), 15% stretched Cu(111), and Cu-terminated CuSn-(0001) surfaces. Energetics calculated with the (a) PW91 and (b) RPBE functionals. The exact numerical values are given in Table 4.

of 1.15[19] and 1.23 Å[20] reported by previous periodic DFT studies.

To demonstrate the differences and similarities in the bonding characteristics of O on these surfaces, electronic density difference plots were generated for O adsorption at the fcc site, which is the preferred site for adsorption of O on Cu(111) and Sn-terminated CuSn(0001) and has energy reasonably close to the preferred site (hcp) on Cu-terminated CuSn(0001) (Figure 6). For both Cu-terminated CuSn(0001) and Sn-terminated CuSn(0001), an increase in the electron density in the p_z orbital of O is observed, whereas there is an electron density depletion in the p_x and p_y orbitals of O. The reverse behavior is observed for O/Cu(111). The stronger binding of O to the Cu-terminated CuSn(0001) surface could be attributed to two factors: (i) the 15% expansive strain in CuSn(0001) lattice as compared to pure Cu(111) and (ii) electronic modification of the Cu surface atoms by subsurface Sn atoms. The binding energy of O on Cu-terminated CuSn(0001) is greater than that on Cu(111) by 17%. Previous studies[19] of the effect of strain on the binding energy of O on Cu(111) show that a 3.8% expansive strain causes the binding energy to increase only by 1.2%. However, our calculations on the 15% stretched Cu(111) surface show that the binding energy of O on this surface is −5.08 [−4.45] eV (Table 4), which is very close to the binding energy observed on the Cu-terminated CuSn(0001) surface. We also find that the site preference for O on Cu(111) changes from the fcc site to the hcp site when 15% strain is induced. Incidentally, the preferred site for O adsorption on Cu-terminated CuSn(0001) surface is also the hcp site. Thus, it appears that as in the case of N, strain is the major factor for enhancement for binding energy of O on the Cu-terminated CuSn(0001) surface, while the electronic effects due to the addition of Sn play only a minor role.

Strong bonding is exhibited by sulfur on Cu-terminated CuSn-(0001) and Cu(111) surfaces. On Cu-terminated CuSn(0001), sulfur prefers the hcp site (binding energy = −5.06 [−4.68] eV as shown in Table 1). The hcp site with a binding energy of

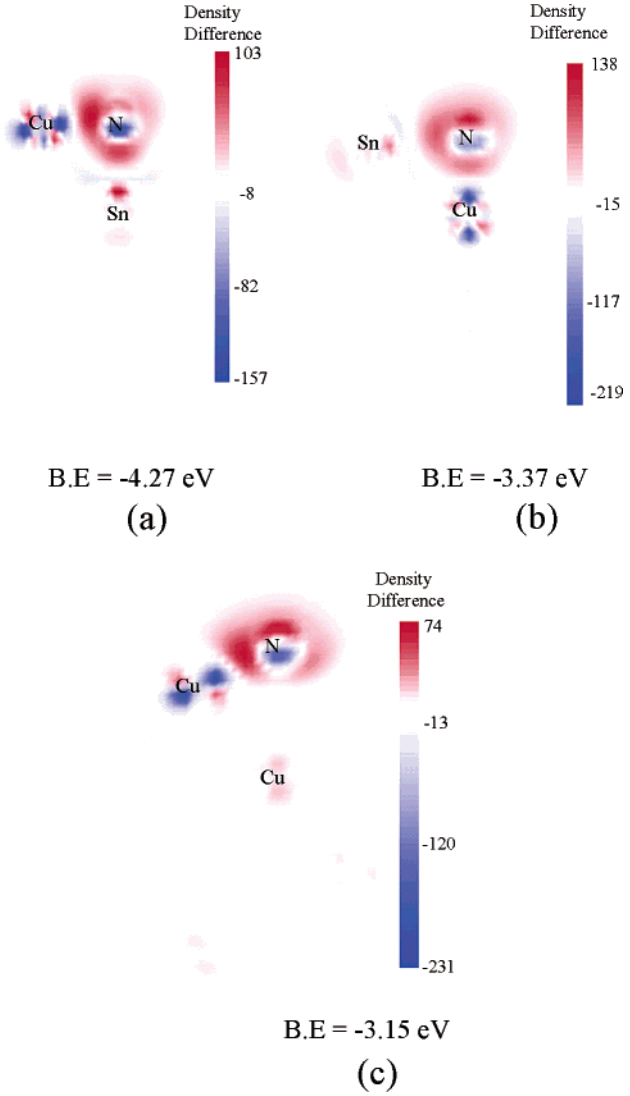

Figure 5. Electron density difference plot for N adsorption at hcp sites on a (a) Cu-terminated CuSn(0001) surface, (b) Sn-terminated CuSn(0001) surface, and (c) Cu(111) surface. Red areas indicate regions of increased electron density, while blue areas indicate regions of electron depletion. The PW91 binding energies for the adsorbed configurations are also shown.

−3.76 [−3.38] eV (Table 1) is also preferred on the Sn-terminated CuSn(0001). On the other hand, on Cu(111), the fcc site, with a binding energy of −4.33 [−3.80] eV (Table 1), is the most favorable site. The binding energies of sulfur and oxygen on Cu-terminated CuSn(0001) and Cu(111) surfaces are very similar. These similarities extend to the characteristics of reconstructions induced by O and S (see Table 3). Table 4 and Figure 4 show that the enhanced binding energy of S on Cu-terminated CuSn(0001) as compared to Cu(111) is caused by both strain and electronic effects. The diffusion barriers for S on Cu-terminated CuSn(0001) and Sn-terminated CuSn(0001) are estimated to be 0.73 [0.71] and 0.66 [0.53] eV, respectively. On Cu(111), the estimated diffusion barrier is only 0.21 [0.10] eV (Table 2) suggesting that S is more mobile on Cu(111) than the CuSn(0001) surfaces. This difference reflects a more corrugated potential energy surface for S on CuSn(0001) as compared to Cu(111).

The most strongly bound atom in the present study is carbon. On both of the Cu-terminated CuSn(0001) and the Sn-terminated CuSn(0001) surfaces, the preferred binding site for C adsorption is the hcp site. The binding energies of C on these surfaces are

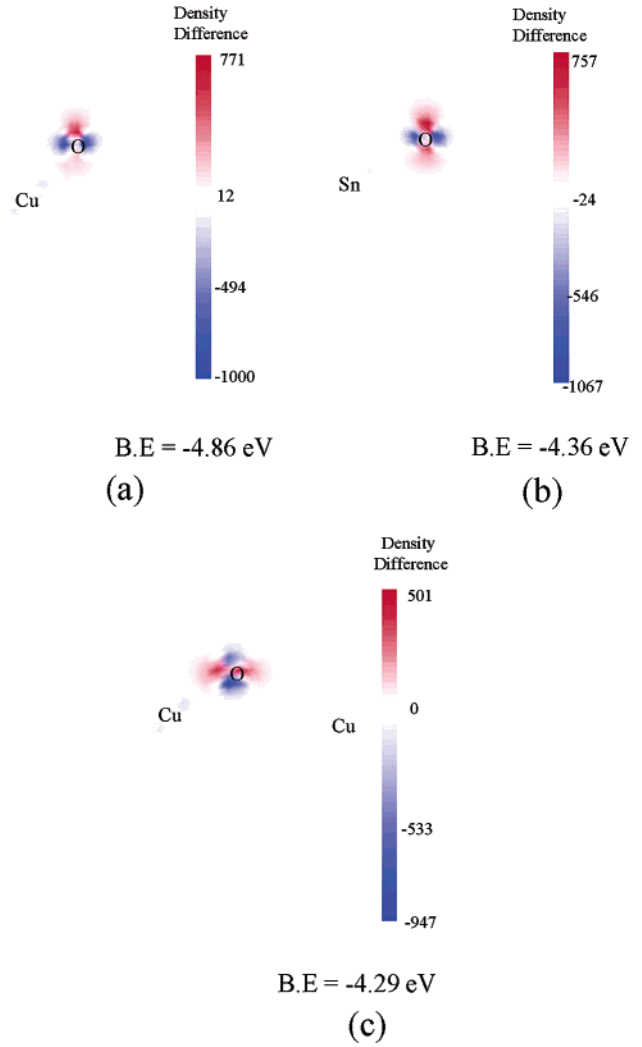

Figure 6. Electron density difference plot for O adsorption at fcc sites on a (a) Cu-terminated CuSn(0001) surface, (b) Sn-terminated CuSn-(0001) surface, and (c) Cu(111) surface. Red areas indicate regions of increased electron density, while blue areas indicate regions of electron depletion. The PW91 binding energies for the adsorbed configurations are also shown.

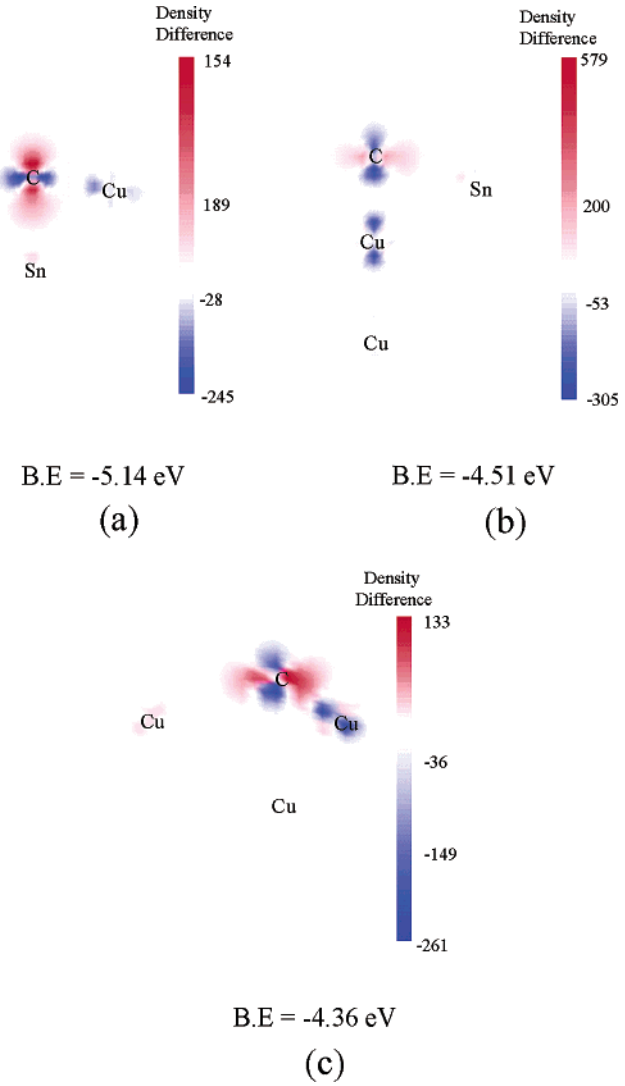

Figure 7. Electron density difference plot for C adsorption at hcp sites on a (a) Cu-terminated CuSn(0001) surface, (b) Sn-terminated CuSn-(0001) surface, and (c) Cu(111) surface. Red areas indicate regions of increased electron density, while blue areas indicate regions of electron depletion. The PW91 binding energies for the adsorbed configurations are also shown.

−5.14 [−4.75] and −4.51 [−4.23] eV, respectively (Table 1).On the other hand, on Cu(111), adsorption of carbon is strongest at the fcc site with a binding energy of −4.41 [−3.90] eV. The geometric parameters of the preferred sites are given in Table 3.

To further analyze the binding of carbon to these surfaces, density difference plots are generated for adsorption at the hcp site. As seen in Figure 7, the stronger binding on the Cu-terminated CuSn(0001) surface is characterized by a strong electron density gain in the p_z orbital of C, whereas in the other two cases, the electron density of that orbital decreases upon adsorption. We also note here that C binds significantly more strongly on a 15% stretched Cu(111) slab than on Cu-terminated CuSn(0001) surface (Table 4 and Figure 4), indicating that addition of Sn to Cu in the Cu-terminated CuSn(0001) tends to decrease the binding of C, while the strain effect tends to enhance binding. The diffusion barrier estimate for C on Cu-terminated CuSn(0001) is 0.63 [0.66] eV, while the barrier on Sn-terminated CuSn(0001) is 0.78 [0.75] eV. On Cu(111), adsorbed C is relatively more mobile, with an estimated diffusion barrier of 0.26 [0.25] eV.

Adsorption of Molecules and Radicals

Nitric oxide (NO) is the least strongly bound of the molecular adsorbates studied on the Cu-terminated CuSn(0001) surface. We find that the magnetic moment of NO is quenched completely on all of the surfaces studied. The best site for NO adsorption on Cu-terminated CuSn(0001) is the bridge site (Figure 3d), with a binding energy of −1.19 [−0.73] eV (Table 1). Adsorbed NO on Cu-terminated CuSn(0001) is tilted with respect to the surface normal by an angle of 14° (Table 5). Similarly, on the Sn-terminated CuSn(0001) surface, NO prefers the bridge-tilted configuration (Figure 3i) and the tilt with respect to the surface normal is 25° (Table 5). The binding energy of NO at this site is −0.65 [−0.35] eV (Table 1). On Cu(111), the best site for NO adsorption is the fcc site with a binding energy of −1.03 [−0.47] eV (Table 1). Our microcalorimetric studies on Cu/SiO_2 show a plateau at 68 kJ/mol (0.70 eV). We note that our microcalorimetric studies have been performed on a supported catalyst, on which the (111) facet may not be the primary surface. Thus, one might suggest that this plateau reflects the binding energy of NO on a stepped surface or other

TABLE 5: Geometric Parameters for Molecular and Radical Adsorbates Adsorbed on Cu-Terminated CuSn(0001), Sn-Terminated CuSn(0001), and Cu(111) Surfaces at Their Preferred Sites[a]

	Cu-terminated CuSn(0001)		Sn-terminated CuSn(0001)		Cu(111)	
adsorbate	bond length (Å)	tilt in degrees	bond length (Å)	tilt in degrees	bond length (Å)	tilt in degrees
NO	1.23	14	1.21	25	1.22	0.0
CO	1.20	0.0	does not adsorb		1.19	0.0
OH	0.98	0.0	0.98	64	0.98	0.0

[a] The bond length gives the atomic distance between the atoms of the adsorbed species. The tilt signifies the angle between the surface normal and the bond axis of the energetically preferred adsorbed states for each species. For comparison, the gas phase bond lengths of NO, CO, and OH are calculated to be 1.19, 1.16, and 0.99 Å, respectively.

less coordinated Cu site as compared to Cu(111). At such a site, the binding energy of NO is expected to be enhanced as compared to the binding energy of −0.47 eV calculated on the Cu(111) surface using the RPBE functional. On the Cu_6Sn_5/SiO_2 catalyst, we find that NO adsorption shows two plateaus at 69 kJ/mol (0.72 eV) and 38 kJ/mol (0.39 eV) (See Figure 1b). Using the RPBE functional, we calculate the binding energy of NO on the Cu-terminated and Sn-terminated CuSn(0001) surfaces to be −0.73 eV and −0.35 eV, respectively. Thus, the binding energies determined using the RPBE functional can be used to explain these experimental results, while the PW91 values tend to overestimate the binding energies. It is noteworthy that the plateau at 0.39 eV, which we attribute to NO adsorption on the Sn-terminated CuSn(0001) surface, is dominant, suggesting that the surface is rich in the Sn-terminated alloy phase.

The results from our DFT calculations show that there is no appreciable change in the bond length of N−O on the three surfaces (Table 5). The preference for adsorption of NO at the fcc site and the perpendicular geometry for NO on Cu(111) are in accord with findings by previous DFT studies,[20] although the binding energy calculated in our work is slightly lower than that determined for a coverage of 1/9 ML on a five layer Cu(111) slab. This lower binding energy is expected, considering that our calculations are performed at higher coverage, where the repulsive interaction between adsorbed NO species is enhanced. Ab initio molecular orbital cluster model studies by Fernadez-Garcia et al.[60] suggest NO to be tilted at 58°, which contradicts our findings. However, IRAS studies by Dumas et al.[61] suggest that NO is perpendicular to the surface in agreement with our findings. Table 4 and Figure 4 show that the binding energies of NO on Cu(111), 15% stretched Cu(111), and Cu-terminated CuSn(0001) surfaces are within 0.20 eV of each other. This result indicates that strain and electronic effects due to Sn addition are less important for NO adsorption than for N adsorption. Furthermore, Table 4 also points out that as in the case of N and O, strain induced by Sn addition is likely to be the main cause for enhancing the binding energy of NO on the Cu-terminated CuSn(0001) surface. The diffusion barriers for NO on the surfaces studied are estimated to be very low (Table 2): (i) less than 0.1 eV on Sn-terminated CuSn(0001), (ii) 0.16-[0.19] eV on Cu-terminated CuSn(0001), and (iii) 0.13 [0.08] eV on Cu(111), identical to the value determined by Bogicevic and Hass.[20]

Carbon monoxide (CO) adsorbs on Cu-terminated CuSn-(0001) and Cu(111) but not on Sn-terminated CuSn(0001). Thus, our experimental observation that negligible amounts of CO adsorb on the Cu_6Sn_5/SiO_2 catalyst indicates that Sn-terminated CuSn is the predominant phase. CO adsorbs strongest on the Cu(111) surface at the fcc and hcp sites with a binding energy

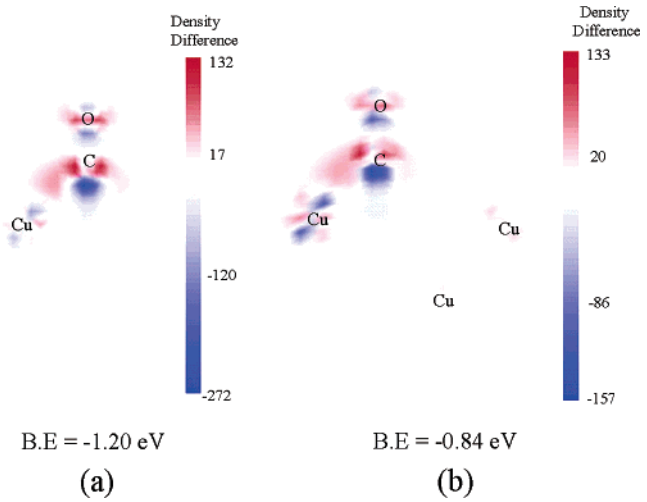

Figure 8. Electron density difference plot for CO adsorption at fcc sites on a (a) Cu-terminated CuSn(0001) surface and (b) Cu(111) surface. Red areas indicate regions of increased electron density, while blue areas indicate regions of electron depletion. The PW91 binding energies for the adsorbed configurations are also shown.

of −0.84 [−0.39] eV (Table 1). The binding energy of CO on Cu-terminated CuSn(0001) is −1.20 [−0.62] eV at the fcc site (see Table 1). The adsorption at the top site of the latter surface is also competitive, with a binding energy of −1.10 [−0.74] eV. Figure 3e,o shows the adsorption of CO at the fcc sites on these surfaces while Tables 3 and 5 give the geometric parameters. Capturing the experimentally determined preferred site (top) for CO adsorption on transition metals represents a well-known, yet unresolved, problem of DFT studies,[5,23] and this difficulty persists in this study as well. Redhead analyses of TPD data typically give binding energies of -0.52 ± 0.05 eV[62,63] for CO adsorbed on the top site on Cu(111). Previous DFT studies[45,64,65] have reported CO binding energies between −0.62 and −0.70 eV at the top site. Our top site binding energy of CO on Cu(111) is −0.73 eV, comparing well with these values. Results from DFT calculations[66] using Cu_{31} clusters suggest a lower binding energy of −0.50 eV at the fcc site. Studies of CO oxidation by Nishiyama et al.[67] have shown that addition of Sn to the surface weakens the adsorption of CO on Rh/SiO_2, indicating that CO does not adsorb on Sn. Similarly, CO oxidation on Pt−Sn alloys appears to be faster than on Pt catalysts, suggesting a weaker metal−CO bond.[68−70] Our studies indicate that CO adsorption on Sn-terminated CuSn(0001) is energetically unfavorable. In addition, the presence of Sn in the second layer at the hcp site of Cu-terminated CuSn(0001) causes CO to bind weakly at this site. The addition of Sn, however, enhances the CO binding at the fcc site of Cu-terminated CuSn(0001). In accord with previous calculations,[45] a considerable fraction of the increase in binding energy on Cu-terminated CuSn(0001) can be attributed to the 15% expansive strain imposed on Cu by alloying it with Sn. Table 4 shows that the binding energy of CO on the 15% stretched Cu(111) slab (−0.99 [−0.58] eV) is significantly higher than the corresponding energy on the equilibrium lattice constant Cu(111) surface. Importantly, the density difference plots in Figure 8 suggest that there is an enhanced donation (charge transfer) to the surface in the case of Cu-terminated CuSn(0001), as compared to Cu(111), whereas back-donation from the surface remains constant, resulting in a stronger bond between the CO and the Cu-terminated CuSn(0001) surface.

The adsorption of hydroxyl (OH) species on Cu-terminated CuSn(0001) is stronger than on Cu(111) or Sn-terminated CuSn-

(0001). The preferred site for OH on Cu-terminated CuSn(0001) is the fcc site, with the OH oriented perpendicular to the surface. The binding energy of OH on this surface is −3.51 [−2.87] eV (Table 1). This is significantly greater than the binding energy of OH on the Sn-terminated surface (−2.76 [−2.37] eV; see Table 1). On the Sn-terminated CuSn(0001) surface, the OH group adsorbs at the top site, tilted with respect to the surface normal at an angle of 64° (see Table 5). The OH species prefers fcc, the perpendicular orientation on Cu(111), and the corresponding binding energy on this surface is −2.85 [−2.26] eV (see Table 1). The geometric parameters for the preferred OH adsorption modes on these three surfaces are given in Tables 3 and 5. The site preference on Cu(111) and the binding energy found for this surface compare reasonably well with findings from previous cluster DFT studies by Koper and van Santen[18] (−3.01 eV) and by Hermann et al.[22] (−2.49 eV). Table 4 and Figure 4 indicate that OH binds considerably more strongly on the 15% stretched Cu(111) surface (−3.34 [−2.82] eV). The stronger interaction of OH with the Cu-terminated CuSn(0001) surface indicates that an electronic effect due to Sn addition is important in enhancing the binding of OH on the Cu-terminated CuSn(0001) surface as compared to the Cu(111) surface. The estimated diffusion barrier for OH on the two CuSn(0001) surfaces and on Cu(111) is very low (see Table 2), suggesting a high mobility of OH on these surfaces.

Thermochemistry of CO, NO, and OH Dissociation and CO Oxidation

Figures 9−11 show the thermochemistry of CO dissociation and CO oxidation, NO dissociation, and OH dissociation on the surfaces studied here. Because CO does not adsorb on Sn-terminated CuSn(0001), the thermochemistry of CO dissociation and CO oxidation reactions was studied only on Cu(111) and Cu-terminated CuSn(0001). The dissociation of CO adsorbed on Cu(111) is highly endothermic and requires 3.11 [3.39] eV. Previous DFT calculations using NLDA pseudopotentials on a Cu_{31} cluster[66] indicate that the energy required for dissociation of adsorbed CO on Cu(111) is 3.69 eV. The dissociation of adsorbed CO on Cu-terminated CuSn(0001) is more favorable (yet still endothermic by 1.98 [2.00] eV) as compared to that on Cu(111), primarily because of the additional stabilization of the products (C and O) on the Cu-terminated CuSn(0001) surface. Thus, as seen from Figure 9, molecular desorption of CO would be preferable to CO dissociation on both surfaces.

Figure 9 also indicates that CO oxidation on Cu(111) and the Cu-terminated CuSn(0001) surface is energetically favorable as compared to CO dissociation. On Cu(111), oxidation of adsorbed CO with surface O is a highly exothermic process with an energy change of −1.02 [−1.72] eV. Previous DFT calculations using cluster methods have shown this reaction to be exothermic by −0.63 eV.[71] Because of the stabilization of CO and O species on the surface, the CO oxidation reaction is less favored on Cu-terminated CuSn(0001), with an energy change of 0.08 [−0.49] eV.

The thermochemical pathway for the adsorption and decomposition of NO to give N and O adsorbed on the surface is depicted in Figure 10. Previous DFT studies on a 3 × 3 unit cell,[20] using PW91, have shown the dissociative adsorption of NO on Cu(111) to be exothermic by 0.79 eV. This value compares well with our predicted thermochemistry on Cu(111), which is exothermic by 0.80 eV. The RPBE functional, however, predicts the reaction to be almost thermoneutral (0.01 eV endothermic). On Sn-terminated CuSn(0001), the reaction is exothermic by 0.99 [0.55] eV, while on Cu-terminated CuSn-

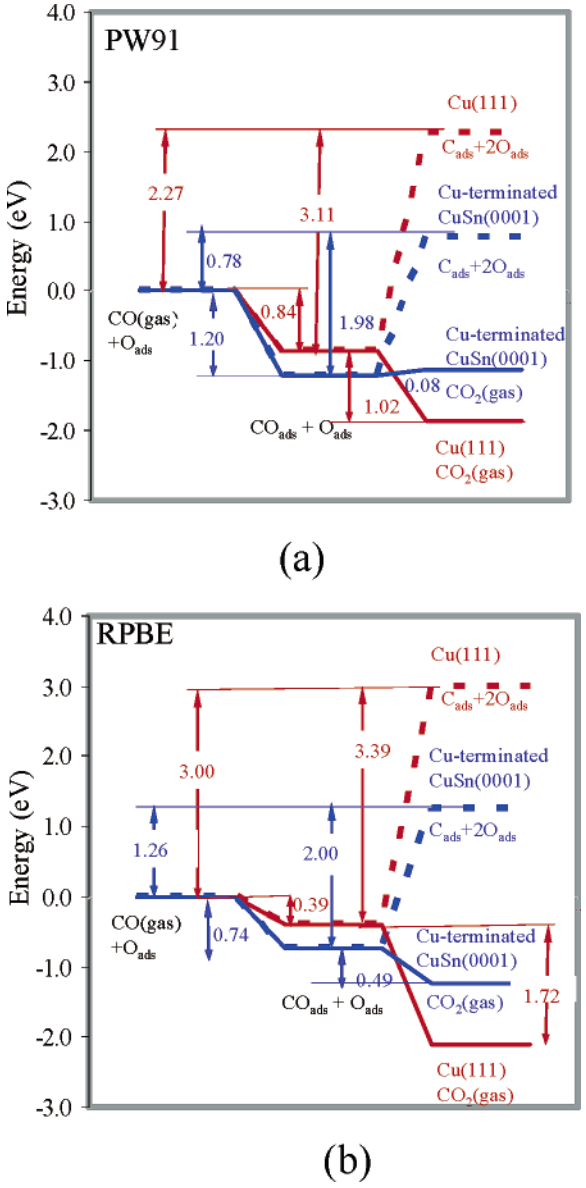

Figure 9. Thermochemistry of CO dissociation and CO oxidation on the Cu-terminated CuSn (0001) and Cu(111) surfaces. The red solid line traces the thermochemical pathway for CO oxidation on Cu(111), while the red dashed line traces the pathway for CO dissociation on Cu(111). Similarly, the solid and the dashed blue lines trace the pathways for CO oxidation and dissociation, respectively, on the Cu-terminated CuSn(0001) surface. The thin lines are a guide to the eye. Reference zero corresponds to the energy of the gas phase CO molecule in the gas phase and an O atom adsorbed on a Cu-terminated CuSn-(0001) or Cu(111) slab at infinite separation from each other. Energetics are calculated with the (a) PW91 and (b) RPBE functionals.

(0001) it is much more exothermic (2.56 [1.99] eV with respect to gas phase NO). The energy for desorption of NO from Cu(111) calculated here (PW91) is 1.03 eV. This is comparable to the reported dissociation barrier of 1.20 eV,[20] suggesting that dissociation and desorption are likely to be competitive. Hence, as suggested by Bogicevic and Haas, NO dissociation can occur on Cu(111) but only at low coverages where site blocking is not predominant.

Our microcalorimetry results show that the heats of NO dissociation on Cu/SiO_2 and Cu_6Sn_5/SiO_2 are −270 (−2.80 eV) and −130 (−1.35 eV) kJ/mol, respectively (Figure 1a,b). The heat of reaction on Cu/SiO_2 is of the same order of magnitude as that for the reaction $NO(g) \rightarrow 1/2N_2(g) + O(a)$ on Cu(111)

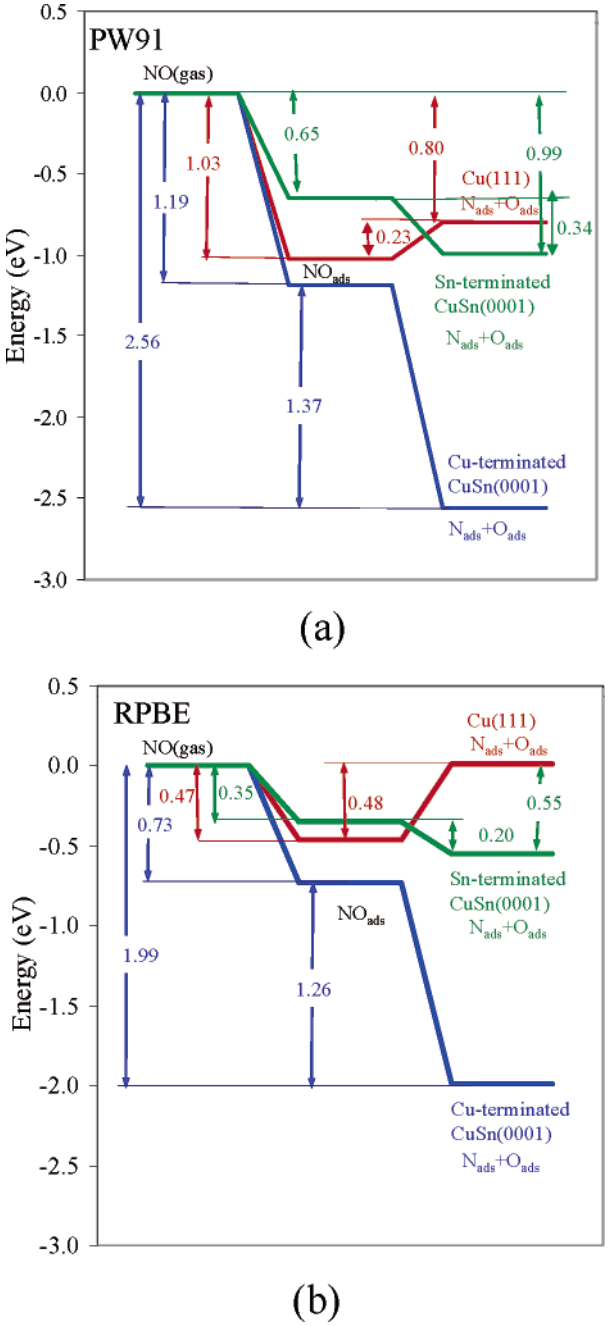

Figure 10. Thermochemistry of NO dissociation on the Cu-terminated CuSn(0001), Sn-terminated CuSn(0001), and Cu(111) surfaces is indicated in blue, green, and red, respectively. The thin lines are a guide to the eye. Reference zero corresponds to the gas phase NO molecule and the corresponding slab at infinite separation. Energetics are calculated with the (a) PW91 and (b) RPBE functionals.

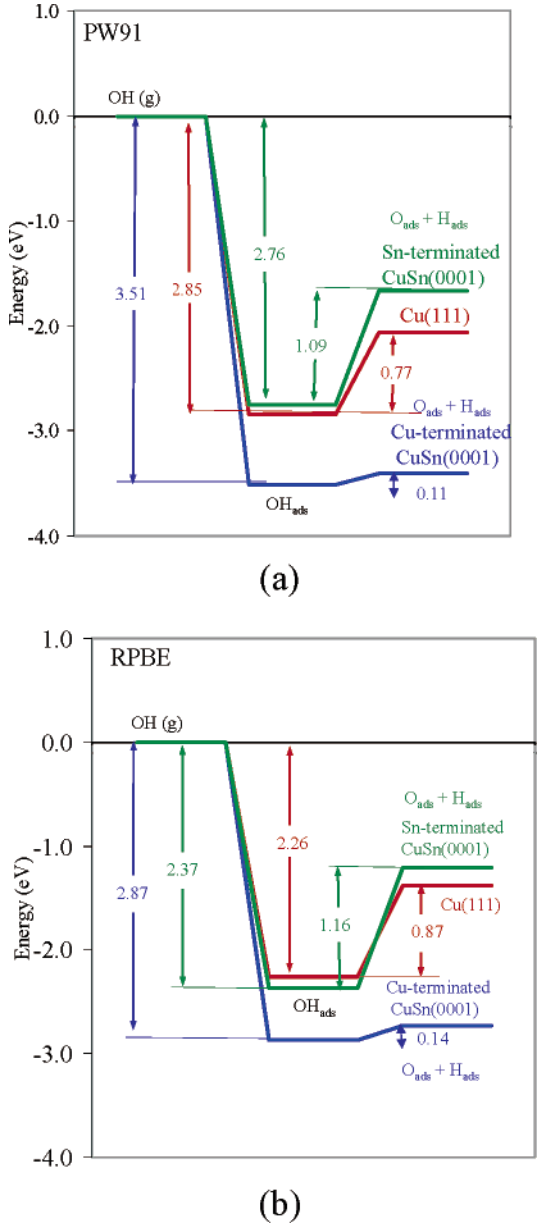

Figure 11. Thermochemistry of OH dissociation on the Cu-terminated CuSn(0001), Sn-terminated CuSn(0001), and Cu(111) surfaces is indicated in blue, green, and red, respectively. The thin lines are a guide to the eye. Reference zero corresponds to the gas phase OH and the corresponding slab at infinite separation. Energetics are calculated with the (a) PW91 and (b) RPBE functionals.

(−2.37 [−1.92] eV). Hence, we suggest that on the Cu/SiO_2 catalyst, NO undergoes dissociation to give N_2 in the gas phase and adsorbed O. Indeed, during the first four doses of NO onto the sample, residual gas was measured in the microcalorimetric cells in an amount consistent with NO dissociation to give gaseous N_2 plus adsorbed oxygen. In contrast, we find that the initial heat of NO reaction on Cu_6Sn_5/SiO_2 is −1.35 eV, which is significantly less than the initial heat on Cu(111). This value is also lower than −2.44 [−2.17] eV, which is the heat of reaction determined for the complete dissociation of NO [NO(g) → 1/2N_2(g) + O(a)]. However, we find that this lower value matches well with the DFT-predicted thermochemistry for the partial dissociation of NO to N_2O [NO(g) → 1/2N_2O(g) + 1/2 O(a)] on the Sn-terminated CuSn(0001) surface (−1.61 [−1.40] eV). Hence, we suggest that the predominant reaction on Cu_6Sn_5/SiO_2 at lower coverages is partial dissociation of NO. Indeed, during the first three doses of NO onto the Cu_6Sn_5/SiO_2 sample, residual gas was measured in the microcalorimetric cells in an amount consistent with NO dissociation to give gaseous N_2O plus adsorbed oxygen. Finally, we suggest that complete dissociation of NO is expected on Cu-terminated CuSn(0001), given the extremely favorable thermodynamics of the NO dissociation reaction on this surface (see Figure 10).

We have also studied the thermochemistry of OH dissociation on Cu-terminated CuSn(0001), Sn-terminated CuSn(0001), and Cu(111). This reaction is of importance for the WGS reaction.[72] This reaction is endothermic on all three surfaces studied (Figure 11). However, OH dissociation is endothermic by only 0.11 [0.14] eV on Cu-terminated CuSn(0001), which is a significant

improvement over Cu(111) (endothermic by 0.77 [0.87] eV). The value for Cu(111) compares well with the energy change predicted by Koper and van Santen[18] (0.67 eV). We find that OH dissociation on Sn-terminated CuSn(0001) is much less favorable (endothermic by 1.09 [1.16] eV), probably because of the lower binding energy of H on this surface.

Conclusions

The adsorption of various atomic (H, O, N, S, and C), molecular (CO and NO), and radical (OH) species on Cu-terminated CuSn(0001), Sn-terminated CuSn(0001), and Cu(111) at 0.25 ML coverage has been studied using periodic, self-consistent DFT calculations. The preferred binding sites for the atomic adsorbates are the 3-fold sites, with the exception of H on Sn-terminated CuSn(0001), where H prefers the top site. This preference for 3-fold sites is found for all molecular adsorbates studied on Cu(111), while certain adsorbates prefer other sites on CuSn(0001) surfaces. In particular, NO prefers bridge-tilted states on CuSn(0001) surfaces, and OH tends to adsorb tilted to the surface at the top site on Sn-terminated CuSn(0001). All adsorbates studied here bind more strongly to the Cu-terminated CuSn(0001) surface than to the Cu(111) surface and to the Sn-terminated CuSn(0001) surface. We suggest that expansive strain in Cu coupled with the electronic structure changes induced by Sn play a significant role in stabilizing most adsorbates on Cu-terminated CuSn(0001).

The thermochemistry of CO dissociation is unfavorable on Cu(111) and Cu-terminated CuSn(0001) surfaces, and molecular desorption is clearly preferred to CO dissociation. On the other hand, thermodynamics favors CO oxidation over molecular desorption of CO on both of the surfaces. Dissociation of OH is endothermic on all three surfaces studied. As compared to the dissociation of CO and OH, NO dissociation thermodynamics are much more favorable on all of the surfaces studied. The energetics of NO dissociation suggests that this reaction is much more feasible on the Cu-terminated CuSn(0001) surface than on Cu(111) and Sn-terminated CuSn(0001) surfaces. Microcalorimetric investigations of NO adsorption and dissociation on a Cu/SiO_2 catalyst indicate that complete NO dissociation to give gaseous N_2 and surface oxygen is favorable on that catalyst. In contrast, on the Cu_6Sn_5/SiO_2 catalyst, which is rich in the Sn-terminated CuSn phase, partial dissociation of NO to give gaseous N_2O plus surface oxygen is favored over complete dissociation to N_2 and adsorbed O.

Acknowledgment. We acknowledge partial financial support from a Catalysis Science Grant (DE-FG-02-03ER15469) provided by the U.S. Department of Energy, Office of Basic Energy Sciences. This research used resources of the National Energy Research Scientific Computing Center, which is supported by the Office of Science of the U.S. Department of Energy under Contract DE-AC03-76SF00098. This research was also performed in part using the Molecular Science Computing Facility (MSCF) in the William R. Wiley Environmental Molecular Sciences Laboratory, a national scientific user facility sponsored by the U.S. Department of Energy's Office of Biological and Environmental Research and located at the Pacific Northwest National Laboratory. We also thank Jeffrey Greeley and Shampa Kandoi for critical reading of the manuscript.

References and Notes

(1) Topsøe, N.-Y.; Topsøe, H. *J. Mol. Catal. A: Chem.* **1999**, *141*, 95.

(2) Fujitani, T.; Nakamura, I.; Uchijima, T.; Nakamura, J. *Surf. Sci.* **1997**, *383*, 285.

(3) Fujitani, T.; Nakamura, K.; Ueno, S.; Uchijima, T.; Nakamura, J. *Appl. Surf. Sci.* **1997**, *121/122*, 583.

(4) Fujitani, T.; Nakamura, J. *Catal. Lett.* **1998**, *56*, 119.

(5) Greeley, J.; Mavrikakis, M. *J. Catal.* **2002**, *208*, 291.

(6) Askgaard, T. S.; Nørskov, J. K.; Ovesen, C. V.; Stoltze, P. *J. Catal.* **1995**, *156*, 229.

(7) Chorkendorff, I.; Niemantsverdriet, H. *Concepts of Modern Catalysis and Kinetics*; Wiley-VCH: Weinheim, 2003.

(8) Lindstrom, B.; Pettersson, L. J. *Int. J. Hydrogen Energy* **2001**, *26*, 923.

(9) Ma, L.; Gong, B.; Tran, T.; Wainwright, M. S. *Catal. Today* **2000**, *63*, 499.

(10) Hansen, J. B. Handbook of Fuel Cells—Fundamentals, Technology, Applications. In *Handbook of Fuel Cells*; Vielstich, W., Lamm, A., Gasteiger, H., Eds.; John Wiley & Sons Ltd.: New York, 2003; Vol. 3, p 141.

(11) Grenoble, D. C.; Estadt, M. M.; Ollis, D. F. *J. Catal.* **1981**, *67*, 90.

(12) Ovesen, C. V.; Stoltze, P.; Nørskov, J. K.; Campbell, C. T. *J. Catal.* **1992**, *134*, 445.

(13) Ovesen, C. V.; Clausen, B. S.; Hammershøi, B. S.; Steffensen, G.; Askgaard, T.; Chorkendorff, I.; Nørskov, J. K.; Rasmussen, P. B.; Stoltze, P.; Taylor, P. *J. Catal.* **1996**, *158*, 170.

(14) Satterfield., C. N. *Heterogeneous Catalysis in Industrial Practice*, 2nd ed.; McGraw-Hill: New York, 1991.

(15) Gates, B. C.; Katzer, J. R.; Schuit, G. C. A. *Chemistry of Catalytic Processes*; McGraw-Hill: New York, 1979.

(16) Thomas, C. L. *Catalytic Processes and Proven Catalysts*; Academic Press: New York, 1970.

(17) Nobuhara, K.; Nakanishi, H.; Kasai, H.; Okiji, A. *J. Appl. Phys.* **2000**, *88*, 6897.

(18) Koper, M. T. M.; van Santen, R. A. *J. Electroanal. Chem.* **1999**, *472*, 126.

(19) Xu, Y.; Mavrikakis, M. *Surf. Sci.* **2001**, *494*, 131.

(20) Bogicevic, A.; Hass, K. C. *Surf. Sci.* **2002**, *506*, L237.

(21) Zeigarnik, A. V.; Valdes-Perez, R. E.; Myatkovskaya, O. N. *J. Phys. Chem. B* **2000**, *104*, 10578.

(22) Hermann, K.; Witko, M.; Pettersson, L. G. M.; Siegbahn, P. *J. Chem. Phys.* **1993**, *99*, 610.

(23) Feibelman, P.; Hammer, B.; Nørskov, J.; Wagner, F.; Scheffler, M.; Stumpf, R.; Watwe, R.; Dumesic, J. *J. Phys. Chem. B* **2001**, *105*, 4018.

(24) Stagg, S. M.; Querini, C. A.; Alvarez, W. E.; Resasco, D. E. *J. Catal.* **1997**, *168*, 75.

(25) Mériaudeau, P.; Naccache, C.; Thangaraj, A.; Bianchi, C. L.; Carli, R.; Vishvanathan, V.; Narayanan, S. *J. Catal.* **1995**, *154*, 345.

(26) Cortright, R. D.; Dumesic, J. A. *J. Catal.* **1995**, *157*, 576.

(27) Watwe, R. M.; Cortright, R. D.; Mavrikakis, M.; Nørskov, J. K.; Dumesic, J. A. *J. Chem. Phys.* **2001**, *114*, 4663.

(28) Agnelli, M.; Candy, J. P.; Basset, J. M.; Bournonville, J. P.; Ferretti, O. A. *J. Catal.* **1990**, *121*, 236.

(29) Candy, J. P.; Ferretti, O. A.; Mabilon, G.; Bournonville, J. P.; Mansour, A. E.; Basset, J. M.; Martino, G. *J. Catal.* **1988**, *112*, 210.

(30) Piccirilli, A.; Pouilloux, Y.; Barrault, J. In *Catalysis of Organic Reactions*; Malz, R. E., Ed.; Marcel Dekker: New York, 1996; p 355.

(31) Grootendorst, E. J.; Pestman, R.; Koster, R. M.; Ponec, V. *J. Catal.* **1994**, *148*, 261.

(32) Harrison, P. G.; Bailey, C.; Daniell, W.; Zhao, D.; Ball, I. K.; Goldfarb, D.; Lloyd, N. C.; Azelee, W. *Chem. Mater.* **1999**, *11*, 3643.

(33) Spiewack, B. E.; Shen, J.; Dumesic, J. A. *J. Phys. Chem.* **1995**, *99*, 17640.

(34) Spiewack, B. E.; Dumesic, J. A. *Thermochim. Acta* **1996**, *290*, 43.

(35) Lund, C. R. F.; Schorfheide, J. J.; Dumesic, J. A. *J. Catal.* **1979**, *57*, 105.

(36) Hammer, B.; Hansen, L. B.; Nørskov, J. K. *Phys. Rev. B* **1999**, *59*, 7413.

(37) Greeley, J.; Nørskov, J. K.; Mavrikakis, M. *Annu. Rev. Phys. Chem.* **2002**, *53*, 319.

(38) Neugebauer, J.; Scheffler, M. *Phys. Rev. B* **1992**, *46*, 16067.

(39) Vanderbilt, D. *Phys. Rev. B* **1990**, *41*, 7892.

(40) Chadi, D. J.; Cohen, M. L. *Phys. Rev. B* **1973**, *8*, 5747.

(41) Perdew, J. P.; Chevary, J. A.; Vosko, S. H.; Jackson, K. A.; Pederson, M. R.; Singh, D. J.; Fiolhais, C. *Phys. Rev. B* **1992**, *46*, 6671.

(42) White, J. A.; Bird, D. M. *Phys. Rev. B* **1994**, *50*, 4954.

(43) Kresse, G.; Furthmuller, J. *Comput. Mater. Sci.* **1996**, *6*, 15.

(44) Villers, P.; Calvert, L. D. *Pearson's Handbook of Crystallographic Data for Intermetallic Phases*, 2 ed.; ASTM International: Newbury, OH, 1991.

(45) Greeley, J.; Gokhale, A. A.; Kreuser, J.; Dumesic, J. A.; Topsøe, H.; Topsøe, N.-Y.; Mavrikakis, M. *J. Catal.* **2003**, *213*, 63.

(46) Xu, Y.; Mavrikakis, M. *Surf. Sci.* **2003**, *538*, 219.

(47) *CRC Handbook of Chemistry and Physics*, 76th ed.; CRC Press: New York, 1996.

(48) Mavrikakis, M.; Rempel, J.; Greeley, J.; Hansen, L. B.; Nørskov, J. K. *J. Chem. Phys.* **2002**, *117*, 6737.

(49) Krekelberg, W. P.; Greeley, J.; Mavrikakis, M. *J. Phys. Chem. B* **2004**, *108*, 987.
(50) Mills, G.; Jonsson, H.; Schenter, G. K. *Surf. Sci.* **1995**, *324*, 305.
(51) Mavrikakis, M.; Hammer, B.; Nørskov, J. K. *Phys. Rev. Lett.* **1998**, *81*, 2819.
(52) Wintterlin, J.; Zambelli, T.; Trost, J.; Greeley, J.; Mavrikakis, M. *Angew. Chem., Int. Ed.* **2003**, *42*, 2850.
(53) Schlapka, A.; Lischka, M.; Gross, A.; Kasberger, U.; Jakob, P. *Phys. Rev. Lett.* **2003**, *91*, 16101.
(54) McCash, E. M.; Parker, S. F.; Pritchard, J.; Chesters, M. A. *Surf. Sci.* **1989**, *215*, 363.
(55) Lamont, C. L.; Persson, B. N. J.; Williams, G. P. *Chem. Phys. Lett.* **1995**, *243*, 429.
(56) Lee, G.; Plummer, E. W. *Surf. Sci.* **2002**, *498*, 229.
(57) Feibelman, P. J.; Hamann, D. R. *J. Vac. Sci. Technol., A* **1987**, *5*, 424.
(58) Stromquist, J.; Bengtsson, L.; Persson, M.; Hammer, B. *Surf. Sci.* **1998**, *397*, 382.
(59) Hammer, B.; Nørskov, J. K. In *Chemisorption and Reactivity on Supported Clusters and Thin Films*; Lambert, R. M., Pacchioni, G., Eds.; Kluwer Academic Publishers: Dordrecht, 1997; Vol. 331, p 285.
(60) Fernandez-Garcia, M.; Conesa, J. C.; Illas, P. *Surf. Sci.* **1993**, *280*, 441.
(61) Dumas, P.; Suhren, M.; Chabal, Y. J.; Hirshmugl, C. J.; Williams, G. P. *Surf. Sci.* **1997**, *371*, 200.
(62) Kirstein, W.; Krüger, B.; Thieme, F. *Surf. Sci.* **1986**, *176*, 505.
(63) Bönicke, I.; Kirstein, W.; Spinzig, S.; Thieme, F. *Surf. Sci.* **1994**, *313*, 231.
(64) Hammer, B.; Morikawa, Y.; Nørskov, J. K. *Phys. Rev. Lett.* **1996**, *76*, 2141.
(65) Zhang, C. J.; Baxter, R. J.; Hu, P.; Alavi, A.; Lee, M.-H. *J. Chem. Phys.* **2001**, *115*, 5272.
(66) van Daelen, M. A.; Li, Y. S.; Newsam, J. M.; van Santen, R. A. *J. Phys. Chem.* **1996**, *100*, 2279.
(67) Nishiyama, S.; Akemoto, M.; Yamamoto, I.; Tsuruya, S.; Masai, M. *J. Chem. Soc., Faraday Trans.* **1992**, *88*, 3483.
(68) Shubina, T. E.; Koper, M. T. M. *Electrochim. Acta* **2002**, *47*, 3621.
(69) Paffett, M. T.; Gebhard, S. C.; Windham, R. G.; Koel, B. E. *J. Phys. Chem. B* **1990**, *94*, 6831.
(70) Hayden, B. E.; Rendall, M. E. *J. Am. Chem. Soc.* **2003**, *125*, 7738.
(71) Wang, G.-C.; Jiang, L.; Pang, X.-Y.; Cai, Z.-S.; Pan, Y.-M.; Zhao, X.-Z.; Morikawa, Y.; Nakamura, J. *Surf. Sci.* **2003**, *543*, 118.
(72) Campbell, C. T.; Daube, K. A. *J. Catal.* **1987**, *104*, 109.